Earth and Planetary Science Letters 274 (2008) 380–391

Contents lists available at ScienceDirect

Earth and Planetary Science Letters

journal homepage: www.elsevier.com/locate/epsl

The mechanics of continental transforms: An alternative approach with applications to the San Andreas system and the tectonics of California

John P. Platt [a,*], Boris Kaus [a,b], Thorsten W. Becker [a]

[a] Department of Earth Sciences, University of Southern California, Los Angeles, CA 90089-0740, USA
[b] Department of Earth Sciences, ETH Zürich, Zürich, Switzerland

ARTICLE INFO

Article history:
Received 4 April 2008
Received in revised form 20 July 2008
Accepted 25 July 2008
Available online 18 September 2008

Editor: C.P. Jaupart

Keywords:
fault mechanics
continental deformation
transform fault
GPS
seismotectonics

ABSTRACT

Displacement on intracontinental transforms is commonly distributed over a zone several hundred km wide, and may incorporate large regions of transtensional and transpressional strain, but no consensus exists on what controls the distribution and style of this deformation. We model the transform boundary as a weak shear zone of finite length that exerts shear stress on the deformable continental lithosphere on either side. Strain-rate decreases away from the shear zone on a scale related to its length. Force balance in this system requires lateral gradients in shear strain-rate to be balanced by longitudinal gradients in stretching rates, which create zones of lithospheric thickening and thinning distributed anti-symmetrically about the shear zone. Simple analytical estimates, two-dimensional (2D) spectral models, and 2D/3D numerical models are employed to study the spatial scales and magnitudes of the zones of uplift and subsidence. Using reasonable parameter values, the models yield geologically relevant rates. Strain-rate components inferred from the GPS-determined 2-D velocity field, and analysis of seismicity using Kostrov's method, taken together with the geological data on the distribution of active faults, uplift, and subsidence, suggest that the distribution and rates of active deformation in California are consistent with our predictions. This validates the assumptions of the continuum approach, and provides a tool for predicting and explaining the tectonics of California and of other intracontinental transform systems.

1. Introduction

Plate boundaries within continental lithosphere comprise broad zones of distributed deformation, but there is no consensus on what controls the width of the zone, or the distribution of strain within it. Intracontinental transforms are commonly characterized by a single master fault that takes up 50% or more of the displacement rate (e.g., Meade and Hager, 2005; Becker et al., 2005), surrounded by a zone of subsidiary faults and related deformation that can extend up to 200 km on either side (e.g., Luyendyk et al., 1985). The velocity distribution across several major transform faults has been characterized in detail by satellite geodesy, and the generally accepted explanation for the velocity field is the accumulation of interseismic elastic strain around a single master fault with a variable locking depth (e.g., Smith and Sandwell, 2003). This explanation does not address the reasons for the distribution of permanent strain in the system, however, which in several cases is remarkably similar to the present-day velocity field (e.g., Bourne et al., 1998). One approach to understanding how such a zone of distributed strain develops is to treat the continental lithosphere as a sheet of continuously deformable material subject to a velocity boundary condition, representing the effect of the plate boundary. England et al. (1985) showed that the fault-parallel velocity, and hence the shear strain-rate, decay approximately exponentially away from the plate boundary, with a length scale $\lambda = L/(2\pi\sqrt{n})$, where L is the length of boundary and n is the exponent for a power-law rheology. This model predicts velocity distributions broadly consistent with observation (England and Wells, 1991, and it has been adapted to deal with lithosphere of variable strength (Whitehouse et al., 2005).

A more elaborate approach that takes rheological layering in the lithosphere into account was taken by Roy and Royden (2000a,b), who modeled the transform as a discrete fault in rigid mantle lithosphere, overlain by a two-layer viscoelastic crust. The shear strain is diffused within the low-viscosity lower crustal layer in this model, which then drives distributed faulting in the upper crust. These authors show that viscous flow beneath the elastic upper crust can produce a progressively widening zone of distributed faulting at the surface, but their assumption of a discrete plate boundary in the underlying upper mantle appears to be inconsistent with evidence from shear-wave splitting studies (Herquel et al., 1999; Rümpker et al., 2003; Savage et al., 2004; Baldock and Stern, 2005; Becker et al., 2006), which suggest that upper mantle deformation beneath continental transforms may be distributed over zones tens or even hundreds of km wide.

* Corresponding author. Tel.: +1 213 821 1194.
E-mail addresses: john.platt@usc.edu (J.P. Platt), bkaus@usc.edu (B. Kaus), twb@usc.edu (T.W. Becker).

0012-821X/$ – see front matter © 2008 Elsevier B.V. All rights reserved.
doi:10.1016/j.epsl.2008.07.052

In this paper we adapt the length-scales concept for a transform that lies entirely within continental lithosphere. We calculate the way stress, strain-rate and velocity change away from the boundary on either side, and we show that a distinctive pattern of lithospheric thinning and thickening will develop as a result of this process. We start with the thin-sheet approach (e.g., England et al., 1985; Flesch et al., 2000), which considers only vertically integrated mechanical properties, and hence neglects the effects of vertical rheological heterogeneities. The elastic/brittle behavior of the upper crust, for example, will modulate the first-order effects we describe, but 3D visco-elasto-plastic numerical modeling that relaxes the thin-sheet approximations suggests that more complex rheologies are unlikely to alter the key results significantly. We set out the basic physical concept, and illustrate its application using the San Andreas Transform of California as an example.

2. Mechanical description of an intracontinental transform

A homogeneous viscous or elastic material tends to distribute strain over its whole volume. Localization of deformation to define a plate boundary zone suggests weakening, reflecting material changes associated with deformation. Weakening may result from the development of brittle fault zones in the upper crust, but microstructural changes associated with ductile deformation in the lower crust or upper mantle are also likely to contribute. Examples of major strike-slip fault zones that were active at temperatures of >500 °C, characteristic of the middle to lower continental crust, suggest that at this level the width of the resulting zone of high strain is ~20–60 km wide (e.g., Jegouzo, 1980; Corsini et al., 1992). Shear-wave splitting studies in transform zones suggest a similar width for the zone of highest strain in the upper mantle (Herquel et al., 1999; Rümpker et al., 2003; Savage et al., 2004; Baldock and Stern, 2005). We therefore model the transform as a weak shear zone with a width of order 50 km, cutting the whole lithosphere. We assume that the shear stress in this weakened zone is related to its width and to the imposed plate velocity, and that it imposes a shear-stress boundary condition on the surrounding lithosphere.

Where the transform terminates there is likely to be a significant reduction in the transform-parallel shear stress. This is most clearly the case where the transform meets a spreading center, as the San Andreas does in the Gulf of California. The change in orientation of the plate boundary, the change in the type of motion, and the transition from continental to oceanic lithosphere, will all favor a sharp reduction in the shear stress within the continental lithosphere beyond the junction. The situation is different where the transition is to a convergent boundary, as happens at the northern end of the Alpine fault in New Zealand, for example. Shear stress along the obliquely convergent Hikurangi margin is likely to be comparable to that along the Alpine fault itself, and this is expressed in the strike-slip faults that are active in the fore arc behind the subducting margin. Where the transform terminates in a triple junction, the change in character and orientation of the boundaries is in general likely to involve a reduction in shear stress. We discuss this point in relation to the San Andreas transform in Section 4.

If the transform-parallel shear stress is largely limited to the transform itself, the resulting shear force on the plates either side will be supported within the plate interiors by regions of lithosphere with linear dimensions substantially greater than the length of the transform boundary. As a result there will be a progressive decrease in stress and strain-rate away from the boundary on either side. This is the physical principle underlying the length-scales concept articulated by England et al. (1985).

Consider the simplest possible mechanical description of the problem, consisting of a horizontal sheet of homogeneous and isotropic material with free upper and lower surfaces, density ρ, containing a vertical planar shear zone that exerts a constant horizontal shear stress on the surrounding medium (Fig. 1). In the following we use σ for components of the full stress tensor, τ for components of the deviatoric stress tensor, and P for pressure. We treat tensile stresses as positive, so that P is negative, and $\tau_{ij}=\sigma_{ij}+P$. We start with the force-balance equations for creeping flow:

$$\frac{\partial \sigma_{ij}}{\partial x_i} = \rho g_j. \tag{1}$$

In a horizontal sheet of material with upper and lower surfaces free of shear stress, we can assume that shear stresses on horizontal planes are on average zero, and we use the thin-sheet approximation, which allows us to neglect vertical gradients in stress. Using Cartesian coordinates with x parallel to the shear zone, y normal to the shear zone, and z vertical (Fig. 1), the force-balance equations in the x and z directions then reduce to:

$$\frac{\partial \tau_{xx}}{\partial x} + \frac{\partial \tau_{xy}}{\partial y} - \frac{\partial P}{\partial x} = 0, \tag{2}$$

$$\frac{\partial \tau_{zz}}{\partial z} - \frac{\partial P}{\partial z} - \rho g = 0. \tag{3}$$

If we neglect regional gradients in topography or density, we can assume from Eq. (3) that σ_{zz} is constant with x and y, so that:

$$\frac{\partial \sigma_{zz}}{\partial x} = 0 \text{ and hence } \frac{\partial \tau_{zz}}{\partial x} = \frac{\partial P}{\partial x}. \tag{4}$$

Substituting Eq. (4) in Eq. (2) then gives:

$$\frac{\partial \tau_{xy}}{\partial y} + \frac{\partial \tau_{xx}}{\partial x} - \frac{\partial \tau_{zz}}{\partial x} = 0. \tag{5}$$

This expression relates the gradient in shear stress away from the shear zone (as predicted by the length-scales relationship, for

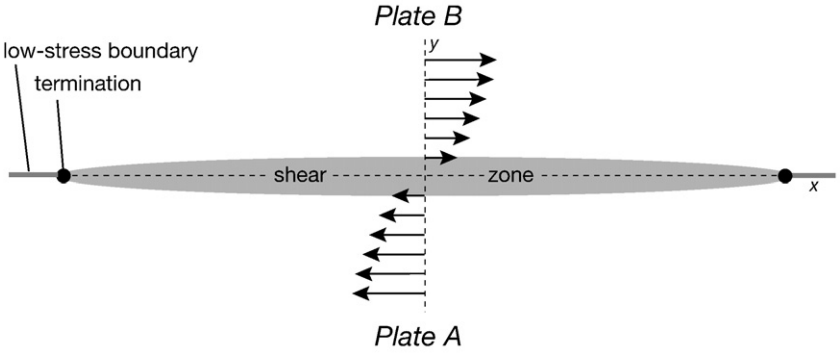

Fig. 1. Geometry and coordinate system for our analysis of a continental transform, treated as a weak shear zone of finite length within deformable continental lithosphere. The shear zone terminates at either end in junctions connecting it to low-strength plate boundaries (the geometry shown is not intended to be realistic). Velocities relative to the average of the two plate velocities are shown schematically on either side of the shear zone, defining velocity profiles of the type predicted by the length-scales model of England et al. (1985).

example) to gradients in deviatoric normal stress parallel to the shear zone. As a result, we might expect components of horizontal extension or contraction parallel to the shear zone. These strains will create topography; in time this will generate stresses that will tend to counteract the effects we describe here (see below).

Assuming that the bounding plates extend for distances normal to the shear zone that are large compared to its length, we can reasonably assume that τ_{yy} is small compared to τ_{xx}, and hence that $\tau_{zz} \approx -\tau_{xx}$. Eq. (5) then reduces to:

$$\frac{\partial \tau_{xx}}{\partial x} \approx -\frac{\partial \tau_{zz}}{\partial x} \approx -\frac{1}{2}\frac{\partial \tau_{xy}}{\partial y}. \tag{6}$$

We can now derive corresponding relations for strain-rate gradients by assuming a constitutive law. If we assume power-law behavior:

$$\tau_{ij} = B E_{II}^{1/n-1} \dot{\varepsilon}_{ij}, \tag{7}$$

where E_{II} is the second invariant of the strain-rate tensor,

$$\frac{\partial \tau_{xx}}{\partial x} = B E_{II}^{1/n-1} \frac{\partial \dot{\varepsilon}_{xx}}{\partial x} + B\dot{\varepsilon}_{xx}(1/n-1)E_{II}^{1/n-2}\frac{\partial E_{II}}{\partial x},$$

$$\frac{\partial \tau_{xy}}{\partial y} = B E_{II}^{1/n-1} \frac{\partial \dot{\varepsilon}_{xy}}{\partial y} + B\dot{\varepsilon}_{xy}(1/n-1)E_{II}^{1/n-2}\frac{\partial E_{II}}{\partial y}.$$

So from Eq. (6):

$$E_{II}\frac{\partial \dot{\varepsilon}_{xx}}{\partial x} + \dot{\varepsilon}_{xx}(1/n-1)\frac{\partial E_{II}}{\partial x} + \frac{1}{2}\left(E_{II}\frac{\partial \dot{\varepsilon}_{xy}}{\partial y} + \dot{\varepsilon}_{xy}(1/n-1)\frac{\partial E_{II}}{\partial y}\right) \approx 0$$

$\dot{\varepsilon}_{xy}$ is the dominant component of strain-rate in a shear zone, so $E_{II} \approx \dot{\varepsilon}_{xy}$, and hence:

$$\dot{\varepsilon}_{xy}\frac{\partial \dot{\varepsilon}_{xx}}{\partial x} + \dot{\varepsilon}_{xx}(1/n-1)\frac{\partial \dot{\varepsilon}_{xy}}{\partial x} + \frac{\dot{\varepsilon}_{xy}}{2n}\frac{\partial \dot{\varepsilon}_{xy}}{\partial y} \approx 0.$$

The middle term is the product of two relatively small terms, so can be neglected, giving:

$$\frac{\partial \dot{\varepsilon}_{xx}}{\partial x} \approx -\frac{\partial \dot{\varepsilon}_{zz}}{\partial x} \approx -\frac{1}{2n}\frac{\partial \dot{\varepsilon}_{xy}}{\partial y} \tag{8}$$

This relationship predicts gradients along the shear zone in the rates of both vertical and horizontal extension or shortening, proportional to the gradients of shear strain-rate normal to the zone. Note that the direction of horizontal extension or shortening created by this effect will be parallel to the shear zone. The extension rate is likely to be around zero near the center of the shear zone, so the gradients will produce fields of horizontal extension and shortening at opposite ends of the shear zone, distributed anti-symmetrically on either side (Fig. 2). These strain fields will be superposed on the overall shear strain associated with the transform boundary.

To get an idea of the magnitude of this effect, we can use the velocity distribution predicted by England et al. (1985) adjacent to the transform boundary:

$$v_x = V_0 \exp\left(-2\pi\frac{\sqrt{n}}{L}y\right) \tag{9}$$

where V_0 is velocity at the boundary and L is the length of the transform.

Hence:

$$\dot{\varepsilon}_{xy} = \frac{1}{2}\frac{\partial v_x}{\partial y} = \frac{-\pi\sqrt{n}}{L}v_x \tag{10}$$

and

$$\frac{\partial \dot{\varepsilon}_{xy}}{\partial y} = \frac{2\pi^2 n}{L^2}v_x \tag{11}$$

So from Eq. (8),

$$\frac{\partial \dot{\varepsilon}_{zz}}{\partial x} = \frac{\pi^2}{L^2}v_x. \tag{12}$$

Integrating Eq. (12) adjacent to the shear zone parallel to x from $x=0$, where the deformation is likely to be close to simple shear and the vertical strain-rate is presumably zero, to its termination, we obtain:

$$(\dot{\varepsilon}_{zz})_{L/2,0} = \frac{\pi^2}{2L}V_0. \tag{13}$$

Note that this rate is independent of either of the rheological parameters (B and n) in the power-law creep Eq. (7), which suggests that the effect we predict is unlikely to be strongly sensitive to the bulk rheology we assume for the lithosphere. We show in Section 4 that for typical values of L and V_0, vertical strain-rates could be of the order of 10^{-15} s^{-1}.

Our prediction is therefore that there will be gradients along the shear zone in the rates of both vertical and horizontal extension or shortening, proportional to the gradients of shear strain-rate normal to the zone; a conclusion alluded to but not developed by England et al. (1985). These gradients will produce fields of horizontal transform-parallel extension and shortening at opposite ends of the shear zone, distributed anti-symmetrically on either side (Fig. 2). The horizontal strains will be associated with vertical thinning or thickening, producing normal or reverse components of motion on faults near the surface, and overall changes in crustal and lithospheric thickness. These strain fields will be superposed on the overall shear strain associated with the transform boundary.

As noted above, this process is self-limiting, as the topographic gradients generated by the deformation will produce stress gradients that will counteract those generated by the transform. If the elevation

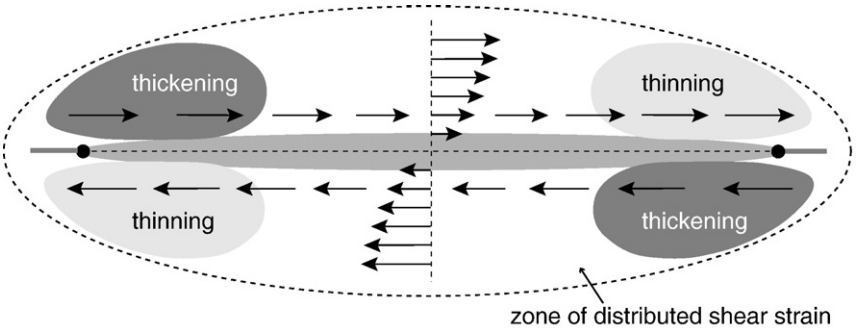

Fig. 2. Velocity distribution parallel to the transform predicted by the force-balance analysis discussed in the text. The velocity gradients shown will result in zones of lithospheric extension and shortening distributed anti-symmetrically about the ends of the shear zone.

difference created along the length of the transform is h, then the longitudinal gradient in the vertical normal stress will no longer be zero, as assumed in Eq. (4), but becomes:

$$\frac{\partial \sigma_{zz}}{\partial x} = \frac{-\rho g h}{L}$$

Eq. (6) then becomes:

$$\frac{\partial \tau_{xx}}{\partial x} \approx -\frac{\partial \tau_{zz}}{\partial x} \approx -\frac{1}{2}\left(\frac{\partial \tau_{xy}}{\partial y} - \frac{\rho g h}{L}\right).$$

The longitudinal normal stress gradients will therefore disappear when:

$$\frac{\partial \tau_{xy}}{\partial y} = \frac{\rho g h}{L} \tag{14}$$

From Eqs. (7), (10), and (11),

$$\frac{\partial \tau_{xy}}{\partial y} = -\tau_{xy}\frac{2\pi}{L\sqrt{n}}$$

so from Eq. (14), longitudinal stress gradients will disappear, and crustal thickening or thinning cease, when:

$$h = \frac{-2\pi \tau_{xy}}{\rho g \sqrt{n}} \tag{15}$$

The negative sign indicates that for a positive (right-lateral) shear stress, h must decrease in the positive x direction. The signs reverse on the opposite side of the fault.

As discussed in Section 4, for likely values of transform-parallel shear stress, h is of the order of several km, suggesting that considerable topography can be generated by this process before it becomes self-limiting.

3. 2D and 3D numerical and analytical modeling

To obtain a more detailed picture of the likely distribution and magnitude of the deformation we predict, we present results from a newly developed 2D spectral semi-analytical solution, from 2D (viscous) finite-element models, and from 3D viscous and visco-elasto-plastic finite-element models (cf. Kaus, 2005; Kaus and Becker, 2007).

3.1. Rheology and methodologies employed

3.1.1. Rheology

In the numerical code employed here, the rheology is assumed to be Maxwell visco-elasto-plastic, where the strain-rate $\dot{\varepsilon}_{ij} = \dot{\varepsilon}_{ij}^{vis} + \dot{\varepsilon}_{ij}^{el} + \dot{\varepsilon}_{ij}^{pl}$. The (linear) viscous part of the deformation $\dot{\varepsilon}_{ij}^{vis} = \tau_{ij}/2\mu$ (μ is viscosity), and the elastic part of the deformation $\dot{\varepsilon}_{ij}^{el} = (D\tau_{ij}/Dt)/2G$ (G is the elastic shear modulus and D/Dt denotes the objective derivative of the stress tensor). If the stress is below the yield strength ($F<0$) the material is viscoelastic, and the plastic part of the deformation $\dot{\varepsilon}_{ij}^{pl} = 0$. The yield function $F = \tau_{II} - P\sin\phi - C\cos\phi$, where $\tau_{II} = \sqrt{\tau_{ij}\tau_{ij}/2}$ is the second invariant of the deviatoric stress tensor, C the cohesion and ϕ the friction angle of brittle rocks (this yield strength envelop mimics the Byerlee strength of upper crustal rocks). If $F>0$, plastic mechanisms are activated and $\dot{\varepsilon}_{ij}^{pl} = \lambda\tau_{ij}/(2|\tau_{II}|)$. λ is found by iterations such that the shear stress is reduced until $\tau_{II} \le \sigma_y = P\sin\phi - C\cos\phi$, and we implicitly assumed a von Mises-type plastic flow potential (Fullsack, 1995; Moresi et al., 2003). In cases where viscous solutions are computed, both the plastic and elastic strain-rates are deactivated.

3.1.2. Spectral, 2D approach

To verify our fully numerical approach, we have developed a 2-D, plane-strain, semi-analytical solution for a finite-thickness variable viscosity weak zone embedded in a matrix of higher viscosity subjected to simple shear boundary conditions. The solution is based on a standard linear perturbation method (Fletcher, 1972, 1977; Johnson and Fletcher 1994; Kaus and Podladchikov, 2001), with the difference that the boundaries between different materials are straight, but the viscosity in the center layer is laterally varying. The derived solutions are for harmonic variations in viscosity, but more realistic variations in viscosity can be applied by means of Fourier superposition.

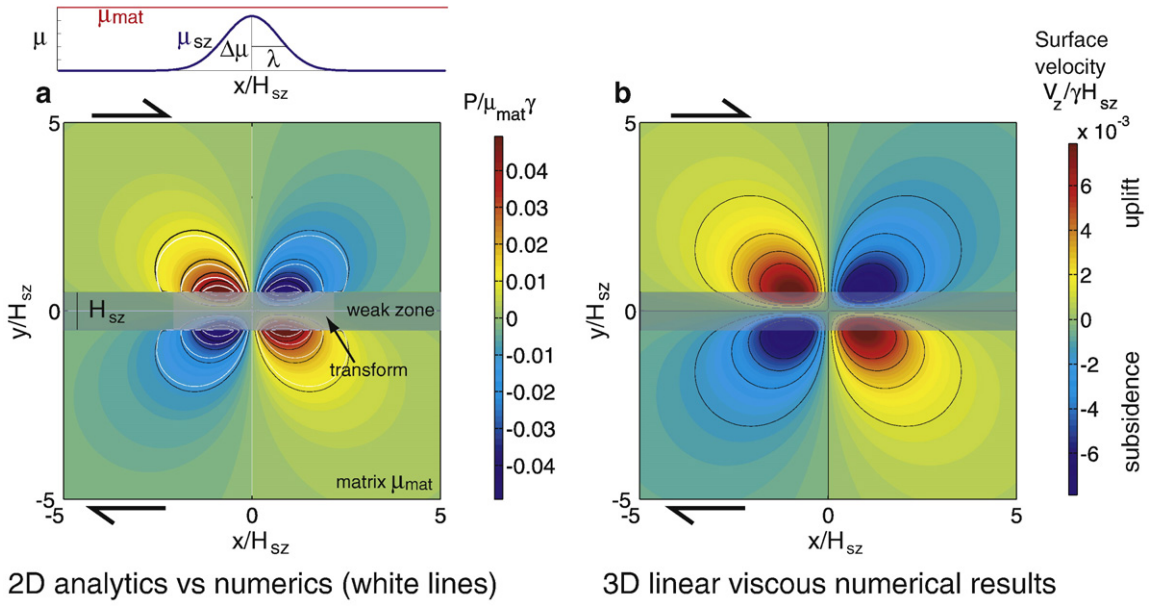

Fig. 3. a) Comparison between analytical and numerical results for 2-D plane-strain deformation in a viscous lithosphere around a weak zone with laterally varying viscosity, given by $\mu = \mu_0 + \Delta\mu\exp(-x^2/\lambda^2)$, as illustrated at the top of the diagram. The section of the weak zone corresponding to the transform is highlighted in grey. Parameters employed are $\mu_0/\mu_{mat} = 0.5$, $\Delta\mu/\mu_{mat} = 0.1$, $\lambda/H_{sz} = 1$. Colors indicate dynamic pressure computed with the analytical model; the solid black and white lines in the top left quadrant highlight the analytical and numerical results respectively. b) Vertical surface velocity in a 3-D numerical model with the same parameters as in (a), in which the upper boundary is a free surface and the thickness of the model is H_{sz}. The effect of gravity is not included in these models.

3.1.3. Numerical finite-element approach

The governing equations are solved with a 3-D Lagrangian finite-element method that employs quadratic shape functions for velocity, and linear discontinuous shape functions for pressure (Cuvelier et al., 1986; Kaus, 2005). Iterations are employed to deal with the non-linearities that result from plasticity, as well as to solve for incompressibility. As boundary conditions, we either employ prescribed velocities (lateral boundaries) or free-slip boundaries, except for the upper boundary which is a free surface in most computations.

The numerical code has been verified versus O-D rheology benchmarks, the 3-D folding instability (Kaus and Schmalholz, 2006), the 2-D viscoelastic Rayleigh–Taylor instability (Kaus and Becker, 2007), and 2-D plane-strain analytical solutions for the current setup (Fig. 2). 2D solutions are computed with the 3D code with one element in the vertical direction and free-slip top and bottom boundary conditions.

3.2. Results

We model the transform boundary as a weak zone that has laterally varying viscosity as shown in Fig. 3a. The shear zone terminates at either end in a triple junction separating it from other types of boundary (represented in the model as zones of still lower viscosity). In order to avoid the singularities that would develop with an abrupt change of viscosity at the terminations of the shear zone, we either vary the viscosity in a Gaussian manner (Fig. 3), or decrease it gradually at the terminations of the shear zone (Fig. 4).

3.2.1. 2D results

Fig. 3a shows that the 2D solutions produce the stress patterns that would be expected from our analytical estimates in Section 2. Comparison between the semi-analytical and numerical results for the 2-D plane-strain case shows good agreement (matching black and white contours in the top left quadrant of Fig. 3a), verifying our finite-element implementation. Imposing a shear velocity on the system results in regions of high and low mean stress (pressure), distributed in an anti-symmetric manner. The absolute value of pressure is a function of the variation in viscosity inside the shear zone, whereas the size of the domains of high and low pressures is proportional to the width of the transform viscosity anomaly.

3.2.2. From 2D to 3D

We performed 3D simulations for the same setup, with the difference that the upper surface was a free surface. The results (Fig. 3b) demonstrate that regions of compression are manifested in surface uplift, whereas regions of extension result in thinning. Fig. 4a shows the result of a simulation in which the viscosity of the weak zone is constant and decreases to a lower value on both sides (representing the terminations of the shear zone). These simulations do not include the effect of gravity: this is taken into account, together with a more complex rheology, next.

The models presented so far assume a homogeneous viscous rheology. Laboratory experiments, however, indicate that brittle (elasto-plastic) deformation mechanisms may be dominant at upper crustal

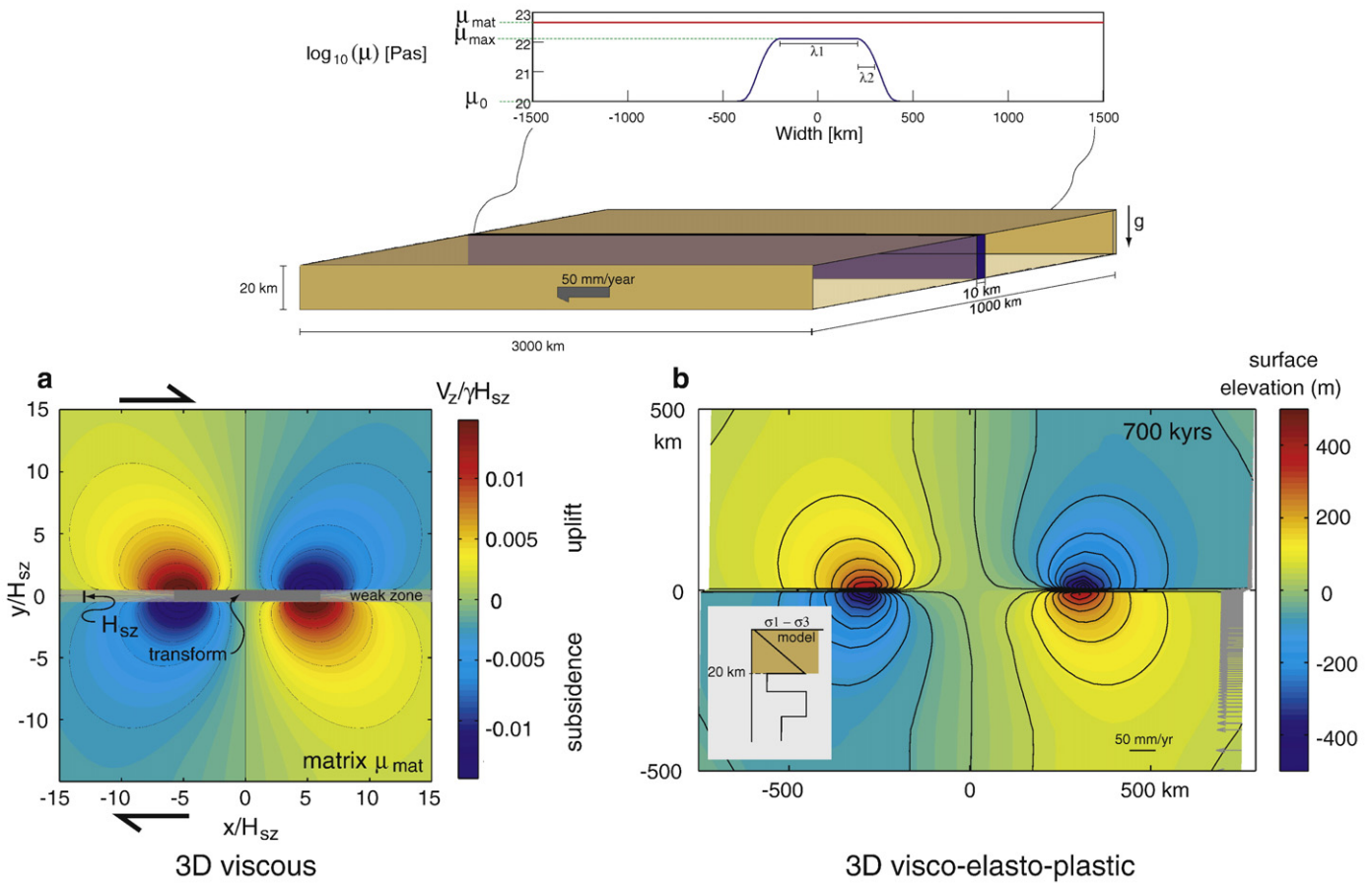

Fig. 4. a) Dimensionless vertical velocity at the free surface around a weak shear zone of width H_{sz} subject to simple shear boundary conditions (computed with a 3D numerical model). The viscosity of the weak zone varies laterally, with maximum value $\mu_{max}/\mu_{mat}=0.2$ for $-2.5H_{sz}<x<2.5H_{sz}$, and with minimum value $\mu_0/\mu_{mat}=0.1$ on either side. Viscosity drops in a Gaussian manner with half-width $\lambda/H_{sz}=3$. Velocity is normalized over the background strain-rate γ inside the weak zone, and the thickness of the model is H_{sz}. b) Surface topography after 700 kyr model evolution in a 3D visco-elasto-plastic model of crustal deformation, subjected to a background simple shear velocity of 50 mm/yr. Model setup is shown on top.

conditions (e.g. Ranalli, 1995; Regenauer-Lieb et al., 2006). Moreover, one could expect that gravity will reduce the vertical motion. For these reasons we have performed a number of more complex numerical simulations in which gravity was activated and we incorporated a visco-elasto-plastic rheology as well as a depth-dependent yield stress. The model setup is shown in Fig. 4 and model parameters are summarized in Table 1. The results (Fig. 4b) show a similar behaviour to that of the 3D viscous model, which leads us to conclude that the phenomena we predict are qualitatively independent of the bulk rheology of the lithosphere. The results also confirm that finite topography can develop in the presence of gravity, and predict gravity to be a limiting factor only for topography on the order of several kms.

4. Application of the model to the San Andreas Transform

The San Andreas Transform is a system of strike-slip faults and related deformation that extends approximately 1200 km along the North American margin, with a displacement rate close to 50 mm/yr. It lies within continental lithosphere except near its northern termination, close to the Mendocino Triple Junction, where it coincides with the boundary between continental and oceanic lithosphere (Melbourne and Helmberger, 2001). Our analysis makes specific predictions about the distribution of transform-parallel extensional and contractional strains that can be tested against observation. The accumulation of finite strain around a transform is complicated by the displacement on the fault itself, however: the crust on either side of the fault, and the terminations of the fault itself, are all in relative motion. Rocks will therefore move through the strain-rate fields we predict, and may move out of them altogether. Transform faults also change their geometry with time: the San Andreas Transform in southern California moved inland from a position along the continental margin to its present location between 6 and 12 Ma (Atwater, 1970; Atwater and Stock, 1998; Wilson et al., 2005), and the location of maximum strain-rate in central and northern California also appears to have moved eastward with time (Wakabayashi, 1999).

For the reasons discussed above we focus here on strain-rate indicators, which should simply reflect the current geometry of the transform. The San Andreas system combines high displacement and high displacement rate with a relatively simple geometry and tectonic setting, and is probably the only system at present where the geodetic and seismotectonic data are sufficiently precise to allow us to test our hypothesis. We must take account, however, of other tectonic processes in California that are largely distinct from the transform system. WNW–ESE oriented extension in the Basin and Range province overlaps the eastern margin of the zone of transform-related shear in eastern California, and the resulting westward component of motion of the Sierra Nevada–Great Valley block is taken up by E–W shortening in the California Coast Ranges (Kreemer and Hammond, 2007). The pattern of deformation in the transform zone has also been strongly influenced by lateral strength contrasts within the North American lithosphere (Le Pichon et al., 2005; Schmalzle et al., 2006; Fialko, 2006), which we have neglected in our analysis. The most obvious of these contrasts is the Sierra Nevada–Great Valley block, which behaves as a large, elongate, essentially rigid block within the transform zone, and as a result has focused transform-related shear into the Eastern California Shear Zone (ECSZ) to the east of it. Whitehouse et al. (2005) demonstrate that the transform-parallel velocity field eastward of the transform can still be modeled using the length-scales concept, if the effect of the rigid block is taken into account. As we discuss below, however, the block creates substantial perturbations of the velocity field at either end, and because its northern termination lies close to the Mendocino triple junction, it complicates interpretation of the northern end of the transform system.

Another important question is how well the San Andreas Transform conforms to our description of a shear zone of finite length cutting continental lithosphere. The transform terminates southward where it meets the East Pacific Rise in the Gulf of California, and geodetic and geologic data suggest that distributed shear does not extend much south of the junction. To the north the transform meets the Cascadia subduction zone at the Mendocino triple junction. Humphreys and Coblentz (2007) suggest that there is a horizontal traction parallel to the Cascadia margin comparable to that exerted by the San Andreas. Juan-de-Fuca–North America plate motion includes a northward component of about 20 mm/yr (McCaffrey et al., 2000), which could generate such a traction. GPS-determined velocities suggest that much of the northward motion is taken up within the Cascadia fore arc, however, and <8 mm/yr of margin-parallel motion is distributed within the North American lithosphere proper (McCaffrey et al., 2000).

In order to identify deformation of the type predicted by our model, we present a simplified analysis of the present-day crustal velocity field in California (Fig. 5). The horizontal GPS velocities from the PBO MIT Joint Network Velocity Solution (2007) are shown with their formal 95% error ellipses in Fig. 5a. We subtracted half of the relative plate motion between the Pacific and North America from NUVEL-1A (DeMets et al., 1994) from the original, stable North America reference frame for visualization purposes. Some of the PBO GPS stations have only been operating for a relatively short time, and velocities are therefore less certain than for older sites, but the PBO velocities have the significant advantage of being part of a consistent network solution for the whole plate boundary. To avoid strain-rate artifacts due to erroneous local velocity estimates, we experimented with variable resolution, damped, uncertainty-weighted spline fits, but found it most straightforward to simply exclude those stations with 1σ errors larger than 2 mm/yr before applying GMT (Wessel and Smith, 1995) splines-under-tension interpolation on a $0.1\times0.1^\circ$ grid. From the interpolated velocity fields we have calculated several functions of the strain-rate tensor, as follows. In Fig. 5b we show the scalar rate of shear strain $e_s=(e_1-e_2)/2$, where e_1 and e_2 are the eigenvalues of the 2-D horizontal strain-rate tensor. This provides a measure of the intensity of shearing, and the maximum intensity may provide a useful indication of the location of the transform at the lithospheric scale, which does not everywhere coincide with the surface trace of the San Andreas Fault. In Fig. 5c we show the mean 2D strain-rate (dilation rate) $e_m=(e_1+e_2)/2$ (Fig. 5c), which is a useful proxy for the vertical strain-rate. In Fig. 5d and e we show the rates of elongation parallel and normal to the plate-motion vector. The latter are defined as the $e_{x'x'}$ and $e_{y'y}$ strain tensor components in a rotated x'–y' coordinate system where x' is oriented locally parallel to the relative Pacific–North America plate motion. Predicted strain-rates rates close to the transform are of the order of the order of 10^{-15} s^{-1}.

Table 1
Symbols and parameters employed in the visco-elasto-plastic simulation

Parameter	Meaning	Employed value
μ_{mat}	Viscosity matrix	5×10^{22} Pa s
μ_0	Minimum viscosity weak zone	10^{20} Pa s
μ_{max}	Maximum viscosity weak zone	10^{22} Pa s
G	Elastic shear modulus	5×10^{10} Pa
ρ	Density	2800 g m^{-3}
g	Gravitational acceleration	10 s^{-2}
C	Cohesion	40 MPa
ϕ	Friction angle	30°
L	Model length	1000 km
W	Model width	3000 km
H	Model height	20 km
H_{sz}	Width of weak zone	10 km
λ_1	Width of maximum viscosity in weak zone	800 km
λ_2	Half-width of Gaussian drop in viscosity	75 km
V_x	Applied shear velocity on front side of model	50 mm/yr
$\dot{\varepsilon}$	Strain-rate	s^{-1}
τ	Deviatoric stress	Pa
P	Pressure	Pa
σ	Stress	Pa

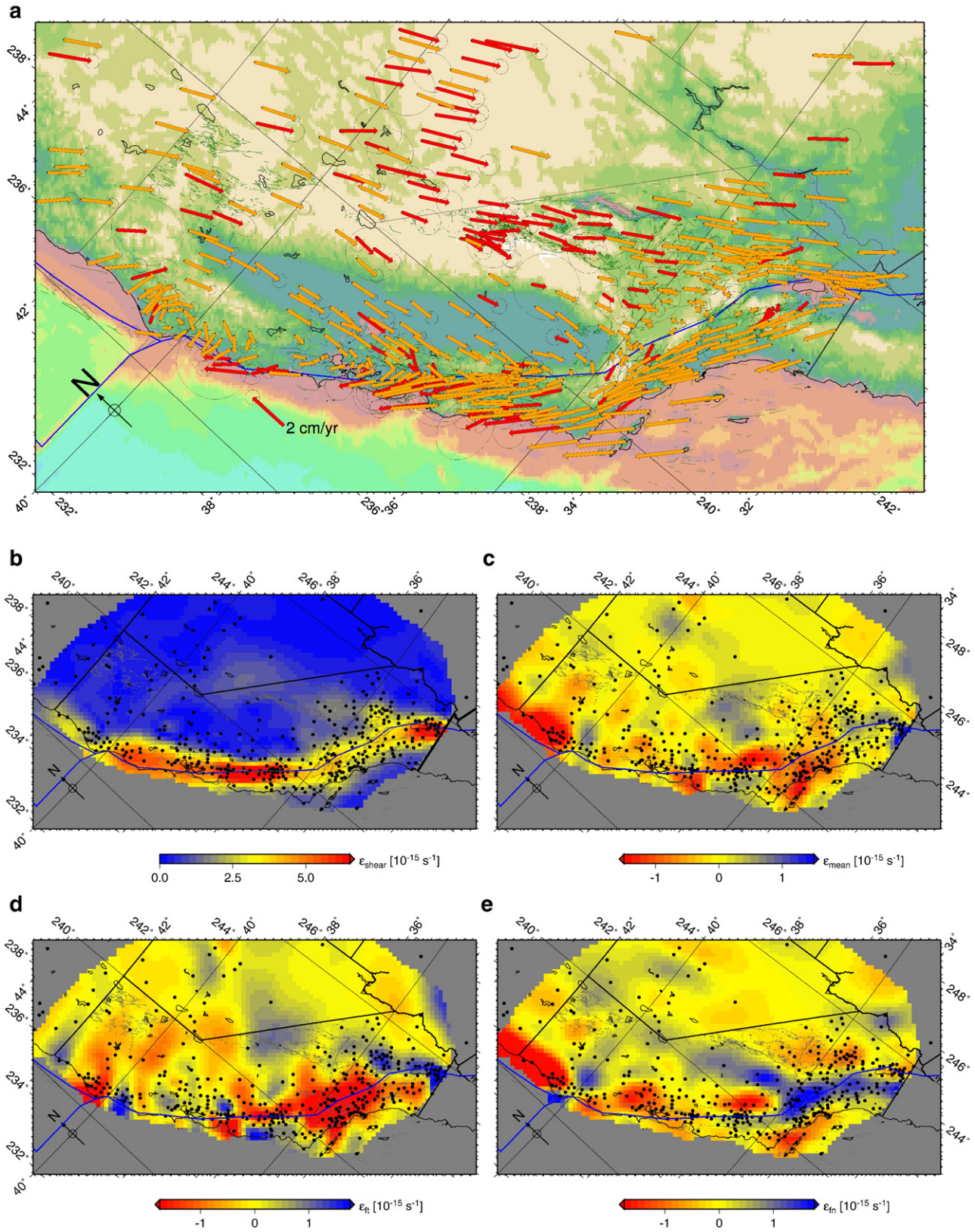

Fig. 5. Velocities and strain-rates in California calculated from the horizontal PBO MIT Joint Network Velocity Solution (2007), plotted on an oblique Mercator projection . (a) Full PBO dataset (red, with 95% error ellipses) and selected velocities (orange, standard deviations smaller than 2 mm/yr). The plate-motion referenced coordinate system was computed by rotating strain-rate tensors according to the local NUVEL1-A plate motion. Coastline and major plate boundary faults shown black, detailed fault strands for California from Jennings (1975) in green. (b) Scalar shear strain-rate. (c) 2-D mean strain-rate (dilation); negative and positive values (red and blue) correspond to thickening and thinning, respectively. (d) plate-motion-parallel elongation rate, (e) plate-motion-normal elongation rate. Estimates (b)–(e) are based on a 0.1 × 0.1° GMT (Wessel and Smith, 1995) interpolation of the selected velocities, the locations of which are indicated by black dots.

We also analyze seismically imaged strain release using the method of Kostrov (1974), i.e. summing up moment tensors derived from focal mechanisms (Fig. 6). Since there is still no homogeneous, state-wide focal mechanism catalog, we merged two existing compilations which are both based on the FPFIT program (Reasenberg and Oppenheimer, 1985). We use the 1964–01/2008 USGS NCSN catalog (2008)

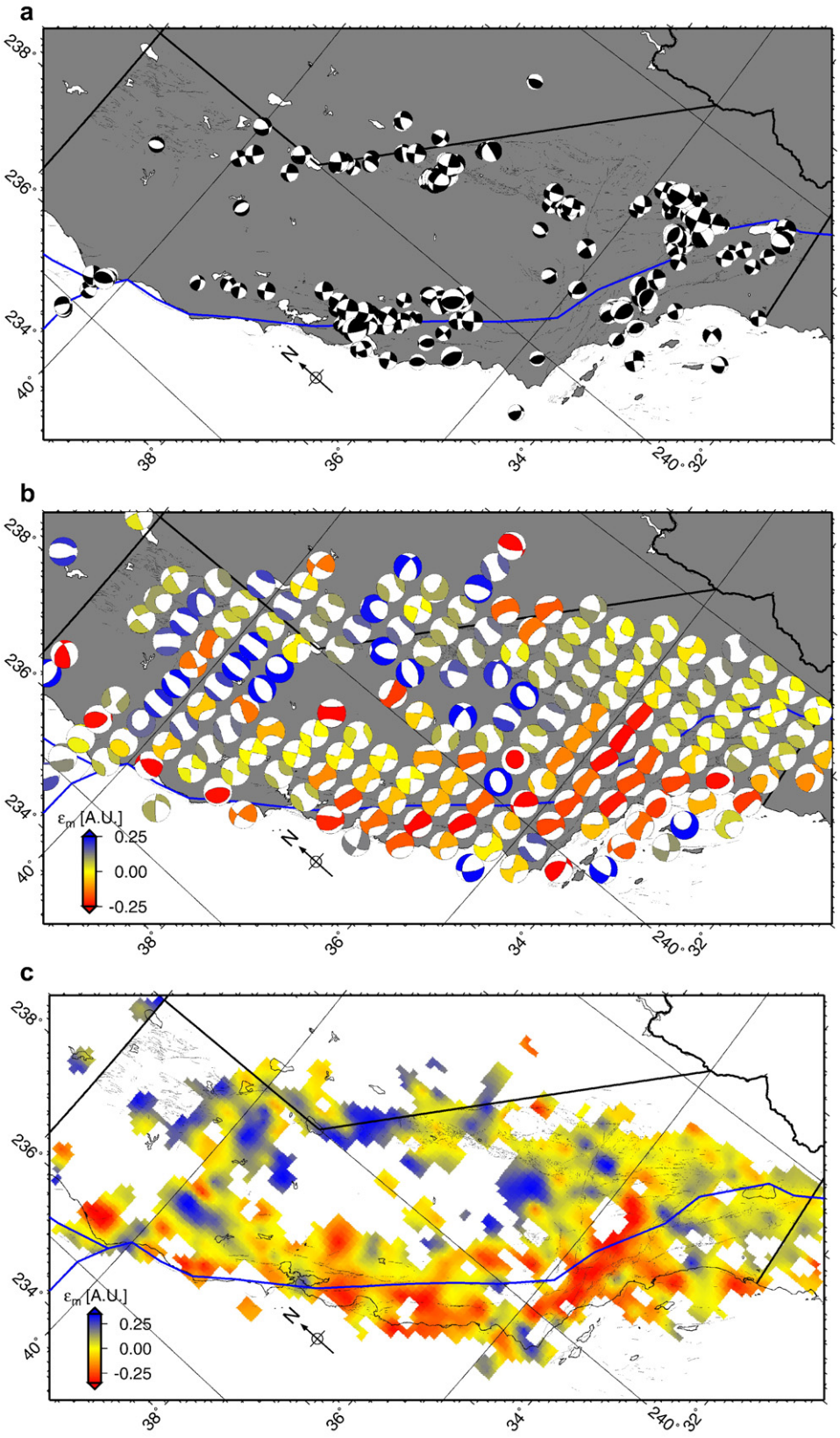

Fig. 6. Analysis of seismic strain release in California using moment tensor summation (Kostrov, 1974) of our merged version of the Hauksson (2000) and USGS NCSN catalog (2008) catalogs. (a) Beach-ball representation (size scales linearly with magnitude) of all individual catalog events with $M_L > 4.5$. (b) CMT style representation of a coarse, normalized Kostrov summation (0.5°×0.5°), shading indicates dilation. (c) dilation of the well-constrained horizontal strain-rate components based on a fine 0.1°×0.1° summation (arbitrary units). We only show regions where a Monte-Carlo estimate of errors in dilation is smaller than 30% of the regional RMS signal.

and the 1975–2000 Hauksson (2000) catalog for northern and southern California, respectively. After selection of high quality focal mechanisms by excluding events with FPFIT misfit>0.2 and station distribution ratios<0.5, and elimination of spatio-temporally close events by favoring the larger magnitude entry, we are left with 74,931 events, all with $M>4.5$ (shown in Fig. 6a).

We then sum the moment tensors for all events with $M>2.5$ on evenly spaced grids assigning each earthquake equal weight ("normalized" summation, Fig. 6b and c). This approach focuses on the geometric style of strain release, rather than the total ("scaled") strain released by earthquakes, which is notoriously affected by the dominance of the large, inadequately sampled events. There are other issues affecting Kostrov analysis, such as the uneven temporal coverage of our merged catalog and uneven magnitude estimates (see, e.g., Bailey et al., submitted for publication). However, those issues will be less important for normalized than for scaled summations, which is why we focus on the former. Fig. 6b shows the summed, tensorial strain on a coarse grid with zero-trace CMT moment tensor symbols, and Fig. 6c the dilational component of the horizontal strain-rates, analogous to the geodetic analysis presented in Fig. 5c. We estimated uncertainties for Fig. 6c by computing 100,000 Monte-Carlo realizations where all input focal mechanisms were rotated by random Gaussian strike, dip, and rake angles with standard deviation of 30°. Fig. 6c shows only those bins where the dilation uncertainty determined in this way was less than 30% of the regional RMS dilation signal.

It is clear that geodesy records mainly interseismic locking, and that seismically recorded strain will be strongly affected by the clustered nature of seismicity. Moreover, image robustness is highly uneven, and both datasets yield few constraints offshore. However, we think that there are certain relatively robust patterns that will likely be confirmed by future, more thorough analysis based on improved datasets. Using these inferences from geodetically and seismically recorded strain-rates together with the topography and the distribution of geologically identifiable active faulting, we discuss the deformation field in a number of clearly identifiable tectonic domains around the transform. In the following discussion, components of velocity and strain-rate parallel to the plate-motion vector are referred to as *transform-parallel*, and components normal to this direction as *transform-normal*. In this sense, parts of the San Andreas Fault are not transform-parallel.

4.1. The Transverse Ranges

The Transverse Ranges are clearly identifiable as a region of crustal thickening and associated surface uplift, and the analysis of the velocity field demonstrates that there is a significant component of transform-parallel shortening and crustal thickening in this area (Fig. 5c and d). This is the area of the WNW-trending "Big Bend" section of the San Andreas fault, and the deformation has generally been attributed to the presence of a large-scale restraining bend in the fault (Hill, 1990). The zone of crustal thickening lies mainly on the SW side of the surface trace of the fault, but locally extends across it into the San Bernadino Mountains (Argus et al., 1999). The seismicity suggests that the dominant deformation is reverse faulting involving N–S shortening, oblique to the plate boundary (Fig. 6b). This deformation field may reflect upper crustal partitioning of the total deformation into components of shortening normal and parallel to the local (WNW) trend of the San Andreas fault, but because the San Andreas fault itself has been aseismic in this region since the 1857 Mw 8.0 Fort Tejon earthquake, a major component of the long term deformation field is missing from the seismic record. Addition of WNW-directed slip on this section of the San Andreas fault would likely bring the seismically recorded deformation field into agreement with the interseismic elastic deformation recorded by the GPS data.

Seismic tomography suggests that deformation in the Transverse Ranges involves the whole crust, and has created an underlying root of thickened lithospheric mantle (Humphreys et al., 1984). The negative buoyancy of this root may be contributing an additional driving force for shortening in this region (Humphreys and Coblentz, 2007).

An additional complication in the area of the Big Bend is revealed by the elongation rate plots, which show a band of transform-normal extension along the trace of the San Andreas Fault in this area (Fig. 5e). This is a result of the deflection of the fault away from the main trend of the plate boundary, so that the elastic strain-rate field associated with the fault is deflected in a counterclockwise sense. The resulting transform-normal extension is not associated with vertical thinning, as can be seen from the dilation plot (Fig. 5c); it reflects the component of horizontal simple shear parallel to the local trace of the fault, and hence there is an equivalent amount of transform-parallel shortening, which in Fig. 5d is partly masked by the transform-parallel shortening and crustal thickening discussed above.

Taken together, the faults in the Transverse Ranges and adjacent areas transfer right-lateral shear deformation WNW, away from the overall trend of the transform system, into the coastal and borderland areas of California. They do this via restraining bends (such as the Big Bend itself), or by trending counterclockwise (and hence in a transpressional orientation) from the plate-motion vector, and the resulting crustal thickening has created the high topography.

We can use Eq. (13) to predict an approximate rate of strain and uplift in this region. Observation suggests that ~50% of the plate motion is accommodated within the Pacific and North American plates on either side of the main fault (e.g., Bourne et al., 1998). If we take $V_0=12.5$ mm/yr, and $L=1200$ km, Eq. (13) predicts a vertical strain-rate of ~50 nanostrains/yr (1.6×10^{-15} s^{-1}) adjacent to the transform near its terminations. Comparable strain-rates are predicted by our numerical models, which are approximately scaled for the San Andreas system, and are of the same order as the strain-rates we calculate from the geodetic data. For a 30 km thick crust, our calculated vertical strain-rate would correspond to rates of thickening or thinning of ~1.5 mm/yr. If the crust is in Airy isostatic compensation, in the absence of erosion or sedimentation the rates of uplift or subsidence would be about 0.23 mm/yr. These rates would decay away from the transform (in the y direction) following the same relationship as in Eq. (9). These are only approximate estimates, but can be compared with the current rate of surface uplift in the Transverse Ranges of California, which, where not affected by erosion, has exceeded 200 m/m.y. over the last few million years (Blythe et al., 2000).

4.2. The Salton Sea Trough and the southern part of the ECSZ

In marked contrast to the transpressional deformation in the Transverse Ranges, active deformation in southeastern California involves substantial crustal thinning. The Salton Sea trough and the adjacent Coachella and Imperial Valleys are extensional basins, as are Owens Valley, Panamint Valley, and Death Valley to the north of the Mojave Desert. Some of these valleys may have been initiated by roughly E–W-directed Basin and Range extension, but in terms of their active deformation, most have been identified as pull-aparts formed along releasing bends on strike-slip faults in the transform system (Burchfiel and Stewart, 1966; Crowell, 1974). The GPS and seismicity show that the entire region is experiencing a combination of transform-parallel extension and dextral slip, and most of it is undergoing crustal thinning (Figs. 5c and d and 6b and c). This is also supported by fault-kinematic data in and around Death Valley, for example (Mcquarrie and Wernicke, 2005; Dewey, 2005). Recent basaltic volcanism over the whole of this region suggests that thinning has involved the whole of the continental lithosphere.

Both the GPS and the seismicity analyses indicate that the Mojave Desert region forms part of this domain of transform-parallel extension (Fig. 5d), but there is considerable uncertainty about how transform-related strain is transferred across this region from the southern San Andreas Fault into the ECSZ further north (Mcquarrie

and Wernicke, 2005). Deformation in this region involves slip on panels of right- and left-lateral faults, accompanied by vertical-axis rotation (Golombek and Brown, 1988; Ross et al., 1989). Given that dextral slip is apparently being transferred across this region in an almost N–S direction, oblique to the trend of the transform, a component of transform-parallel extension is to be expected (Hudnut et al., 2000).

4.3. The northern part of the ECSZ

Geodetic data indicate that 10–12 mm/yr of slip, or ~25% of the total North America–Pacific motion, is transferred along a broad zone of deformation east of the Sierra Nevada separating the Sierra Nevada/Great Valley block from the rest of the Cordillera (Bennet et al., 2003; Meade and Hager, 2005; Becker et al., 2005). As discussed above, the southern part of this zone is transtensional, with a significant transform-parallel component of extension. North of Lake Tahoe, however, the zone of highest strain-rate swings to a more westerly trend, as the displacement associated with the ECSZ is transferred westward towards the Mendocino triple junction (Unruh et al., 2003). The GPS analysis suggests a complicated pattern of strain, with transform-parallel shortening, some transform-normal extension, and minor crustal thickening (Fig. 5). The seismicity shows that deformation is spatially partitioned, with areas dominated by Basin and Range style normal faulting accommodating E–W extension (Surpless et al., 2002; Unruh et al., 2003), interspersed with areas of transpressional and reverse faulting (Fig. 6c). Nearly all these areas show a component of transform-parallel shortening, however, confirming the results of the GPS analysis.

4.4. The California Coast Ranges

Much of the California Coast Ranges is a region of active uplift. The GPS analysis and seismicity show that there is a continuous zone of transform-normal shortening from the western Transverse Ranges into the northern Coast Ranges (Fig. 5e), accompanied by crustal thickening (Figs. 5c and 6c). This is taking up the westerly motion of the Sierra Nevada–Great Valley block, and is ultimately accommodating E–W extension in the Basin and Range province (Prescott et al., 2001). Most of the Coast Ranges also show transform-parallel extension (Fig. 5d), and it is this component of deformation that is of direct relevance to the processes discussed in this paper. Transform-parallel extension is particularly marked in the northern Coast Ranges, where it coincides with a region of eastward-stepping strike-slip faults and associated pull-apart basins, such as San Pablo Bay along the Hayward fault (Jachens and Zoback, 1999; Parsons et al., 2003, 2005).

4.5. The Klamath Mountains

The California Coast Ranges terminate northwards at the transition to the Klamath Mountains, and the GPS analysis indicates a rapid change to transform-parallel shortening associated with this transition (Fig. 5d), associated with crustal thickening (Fig. 5c) (Furlong and Govers, 1999). This area of thickening is clearly distinct from the zone of contraction above the Cascadia subduction zone in the Coast Mountains of Oregon (McCrory, 2000), which is associated with margin-normal contraction on this boundary (Fig. 5e).

4.6. Interpretation

The overall pattern of deformation described from the five regions above is summarized in Fig. 7, and is consistent with our prediction of an anti-symmetric pattern of transform-parallel extension and shortening around the transform (compare Figs. 7 and 1). The Transverse Ranges and adjacent areas in SW California is a region of transform-parallel shortening and crustal thickening that lies in the southern quadrant of the main zone of transform-related deformation, where our analysis would predict it. The strain in this area has clearly been accentuated by the presence of the Sierra Nevada–Great Valley block immediately to the north, the westward motion of which has created the Big Bend in the San Andreas.

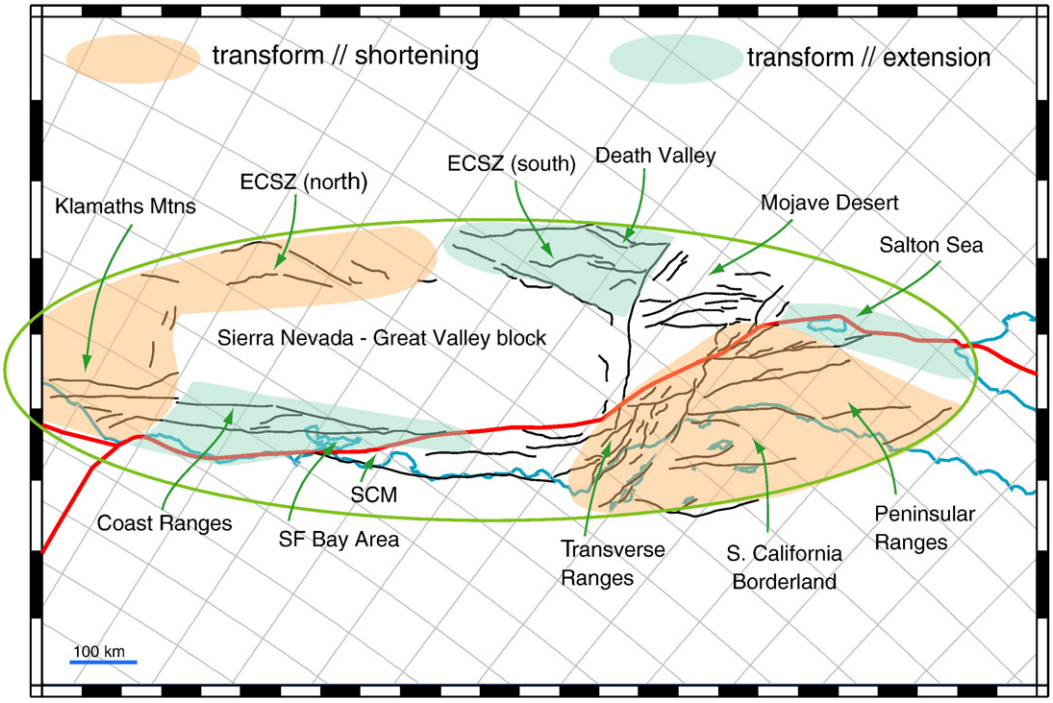

Fig. 7. The San Andreas transform system, plotted on an oblique Mercator projection. The surface expression of the plate boundary is in red; active faults related to present-day plate motion in black. Regions of active crustal thickening and thinning associated with transform-parallel strains, based on the analysis of the velocity data (Fig. 5), seismicity (Fig. 6), and geological data (discussed in the text), are highlighted in orange and green.

The Klamath Mountains and the northern part of the ECSZ define an analogous area of transform-parallel shortening in the northern quadrant of the transform zone (Fig. 7). Again, this in accord with our predictions, but the strain has probably been accentuated by the presence of the Sierra Nevada–Great Valley block to the south.

The pull-apart basins in SE California and the southern part of the ECSZ define an area of transform-parallel extension and crustal thinning in the eastern quadrant of the transform zone (Fig. 7), and the extensional basins in the northern Coast Ranges and the San Francisco Bay area define the equivalent area in the western quadrant. The Coast Ranges present the most problems for our interpretation, in that much of the region of transform-parallel extension lies east of the trace of the San Andreas Fault. A likely explanation for this can be seen on the plot of shear strain-rate (Fig. 5b), which suggests that the locus of highest shear strain-rate passes east of the San Francisco Bay area and up past Clear Lake in the northern Coast Ranges. It is noteworthy that the 50% velocity contour, where the GPS-defined surface velocities are half-way between those of the Pacific and North American plates (Fig. 5a), follows the same trend, approximately along the trace of the Hayward fault and its equivalents further north. In terms of the surface velocities and strain-rates, therefore, the trace of the transform lies well east of the San Andreas fault in the northern Coast Ranges, and hence much of the region of transform-parallel extension does in fact lie west of the transform, where our analysis predicts it should be.

A more general problem is the distortion and modification of the predicted strain field by the rigid Sierra Nevada–Great Valley block, and the westward motion of this block driven by Basin and Range extension. A full analysis of the effect of this block will require more elaborate 3-D modeling, which is beyond the scope of this paper.

The rates of transform-parallel shortening and extension predicted by our model are of the order of 10^{-15} s^{-1}. These are consistent with the approximate rates that we calculate from the GPS data. Hence it appears that our model is capable of explaining many of the characteristic active tectonic and topographic features of California, including crustal thickening in the Transverse Ranges of California, and the extensional basins of southeastern California and the San Francisco Bay area. A significant question, therefore, is whether the topography that has been generated is sufficient to limit further deformation. Humphreys and Coblentz (2007) estimate the shear force parallel to the San Andreas Transform at 1–2 TN per meter length, which corresponds to a shear stress of 16–33 MPa averaged over a 60 km thick mechanical lithosphere. For $n=3$, Eq. (15) then predicts a limiting value of h of 1700–4360 . The actual value of h along the San Andreas transform is around 1500 m, which suggests that it may not yet have reached its limiting value.

5. Conclusions

We have treated an intracontinental transform as a weak shear zone of finite length that imparts a shear stress to the surrounding lithosphere, modeled both as a thin viscous sheet and as a 3-D plate. Our predictions of anti-symmetrically disposed regions of transform-parallel shortening and extension in this situation are consistent with the pattern of active deformation in California, and the strain-rates predicted by our models are consistent with those inferred from our analysis of the present-day velocity field. These successful predictions validate our use of the continuum approximation. Our approach provides a useful tool for predicting and explaining the pattern of deformation around intracontinental transforms.

Acknowledgments

Thanks to Gene Humphreys, Danijel Schorlemmer, Dani Schmid, Frances Cooper, Whitney Behr, and several anonymous reviewers for comments and criticism. Computational work was conducted at the USC Center for High Performance Computing (www.usc.edu/hpcc); some figures were created with GMT (Wessel and Smith, 1995); the velocity solution used data services provided by the Plate Boundary Observatory operated by UNAVCO for EarthScope supported by NSF (No. EAR-0323309), and the research was supported by the Southern California Earthquake Center (SCEC), funded by NSF Cooperative Agreement EAR-0106924 and USGS Cooperative Agreement 02HQAG0008. SCEC contribution number 1109.

References

Argus, D.F., Heflin, M.B., Donnellan, A., Webb, F.H., Dong, D., Hurst, K.J., Jefferson, D.C., Lyzenga, G.A., Watkins, M.M., Zumberge, J.F., 1999. Shortening and thickening of metropolitan Los Angeles measured and inferred by using geodesy. Geology 27, 703–706.

Atwater, T.M., 1970. Implications of plate tectonics for the Cenozoic tectonic evolution of western North America. Geol. Soc. Amer. Bull. 81, 3513–3536.

Atwater, T.M., Stock, J.M., 1998. Pacific–North America plate tectonics of the Neogene southwestern United States—an update. Int. Geol. Rev. 40, 375–402.

Bailey, I., Becker, T. W., and Ben-Zion, Y., submitted for publication, Patterns of co-seismic strain computed from southern California focal mechanisms: Submitted to Geophysical Journal International. Available online at http://geodynamics.usc.edu/~becker/preprints/bbb08.pdf.

Baldock, G., Stern, T., 2005. Width of mantle deformation across a continental transform: evidence from upper mantle (Pn) seismic anisotropy measurements. Geology 33, 741–744.

Becker, T.W., Hardebeck, J.L., Anderson, G., 2005. Constraints on fault slip rates of the southern California plate boundary from GPS velocity and stress inversions. Geophys. J. Int. 160, 634–650.

Becker, T.W., Schulte-Pelkum, V., Blackman, D.K., Kellogg, J.B., O'Connell, R.J., 2006. Mantle flow under the western United States from shear wave splitting. Earth Planet. Sci. Lett. 247, 235–251.

Bennet, R.A., Wernicke, B.P., Niemi, N.A., Friedrich, A.M., 2003. Contemporary strain rates in the northern Basin and Range province from GPS data. Tectonics 22, 1008. doi:10.1029/2001TC001355.

Blythe, A.E., Burbank, D.W., Farley, K.A., Fielding, E.J., 2000. Structural and topographic evolution of the Central Transverse Ranges, California, from apatite fission-track, (U–Th)/He and digital elevation model analyses. Basin Res. 12, 97–114.

Bourne, S.J., England, P.C., Parsons, B., 1998. The motion of crustal blocks driven by flow of the lower lithosphere and implications for slip rates of continental strike-slip faults. Nature 391, 655–660.

Burchfiel, B.C., Stewart, J.H., 1966. "Pull-apart" origin of the central segment of Death Valley, California. Geol. Soc. Amer. Bull. 77, 439–442.

Corsini, M., Vauchez, A., Archanjo, C., de Sá, E.F.J., 1992. Strain transfer at continental scale from a transcurrent shear zone to a transpressional fold belt: the Patos–Seridó system, northeastern Brazil. Geology 19, 586–589.

Crowell, J.C., 1974. Origin of late Cenozoic basins in Southern California. In: Dickinson (Ed.), Tectonics and Sedimentation. Society of Economic Paleontologists and Mineralogists Special Publication, vol. 22, pp. 190–204.

Cuvelier, C., Segal, A., van Steemhoven, A., 1986. Finite Element Methods and Navier–Stokes Equations, Mathematics and Its Applications. Reidel Publishing Company, Dordrecht.

DeMets, C., Gordon, R.G., Argus, D.F., Stein, S., 1994. Effect of recent revisions to the geomagnetic reversal time scale on estimates of current plate motions. Geophys. Res. Lett. 21, 2191–2194.

Dewey, J.F., 2005. Transtension in the Coso region of the central Basin and Range. Occasional Papers of the Geological Institute of Hungary, vol. 204, pp. 9–19.

England, P.C., Wells, R.E., 1991. Neogene rotations and quasicontinuous deformation of the Pacific Northwest continental margin. Geology 19, 978–981.

England, P., Houseman, G., Sonder, L., 1985. Length scales for continental deformation in convergent, divergent, and strike-slip environments: analytical and approximate solutions for a thin viscous sheet model. J. Geophys. Res. 90, 3551–3557.

Fialko, Y., 2006. Interseismic strain accumulation and the earthquake potential on the southern San Andreas fault system. Nature 441, 968–971. doi:10.1038/nature04797.

Flesch, L.M., Holt, W.E., Haines, A.J., Shen-Tu, B., 2000. Dynamics of the Pacific–North American plate boundary in the Western United States. Science 287, 834–836.

Fletcher, R.C., 1972. Application of a mathematical model to emplacement of mantled gneiss domes. Am. J. Sci. 272, 197–216.

Fletcher, R.C., 1977. Folding of a single viscous layer—exact infinitesimal amplitude solution. Tectonophysics 39, 593–606.

Furlong, K., Govers, R., 1999. Ephemeral crustal thickening at a triple junction: the Mendocino crustal conveyor. Geology 27, 127–130.

Fullsack, P., 1995. An Arbitrary Lagrangian–Eulerian formulation for creeping flows and its application in tectonic models. Geophys. J. Int. 120, 1–23.

Golombek, M., Brown, L., 1988. Clockwise rotation of the western Mojave Desert. Geology 16, 126–130.

Hauksson, E., 2000. Crustal structure and seismicity distribution adjacent to the Pacific and North America plate boundary in southern California. J. Geophys. Res. 105, 13,875–13,903.

Herquel, G., Tapponnier, P., Wittlinger, G., Mei, J., Danian, S., 1999. Teleseismic shear wave splitting and lithospheric anisotropy beneath and across the Altyn Tagh fault. Geophys. Res. Lett. 26, 3225–3228.

Hill, M.L., 1990. Transverse Ranges and neotectonics of southern California. Geology 18, 23–25.

Hudnut, K.W., King, N.E., Galetzka, J.E., Stark, K.F., Behr, J.A., Aspiotes, A., van Wyk, S., Moffit, R., Dockter, S., Wyatt, F., 2002. Continuous GPS observations of postseismic deformation following the 16 October 1999 Hector Mine, California, earthquake (Mw 7.1). Bull. Seismol. Soc. Am. 92, 1403–1422.
Humphreys, E.D., Coblentz, D.D., 2007. North American dynamics and western U.S. tectonics. Rev. Geophys. 45, RG3001 8755-1209/07/2005RG000181.
Humphreys, E., Clayton, R.W., Hager, B.H., 1984. A tomographic image of mantle structure beneath southern California. Geophys. Res. Lett. 11, 625–627.
Jachens, R.C., Zoback, M.L., 1999. The San Andreas Fault in the San Francisco Bay region, California; structure and kinematics of a young plate boundary. Int. Geol. Rev. 41, 191–205.
Jegouzo, P., 1980. The South Armorican shear zone. J. Struct. Geol. 2, 39–48.
Jennings, C.W., 1975, Fault map of California with locations of volcanoes, thermal springs, and thermal wells: California Division of Mines and Geology California Geologic Data Map 1, scale 1:750,000.
Johnson, A.M., Fletcher, R.C., 1994. Folding of Viscous Layers: Mechanical Analysis and Interpretation of Structures in Deformed Rocks. Columbia University Press, New York, New York. 461 pp.
Kaus, B.J.P., 2005, Modelling approaches to geodynamic processes, PhD-thesis, Swiss Federal Institute of Technology.
Kaus, B.J.P., Podladchikov, Y.Y., 2001. Forward and reverse modeling of the three-dimensional viscous Rayleigh–Taylor instability. Geophys. Res. Lett 28, 1095–1098.
Kaus, B.J.P., Schmalholz, S.M., 2006. 3D finite amplitude folding: implications for stress evolution during crustal and lithospheric deformation. Geophys. Res. Lett. 33 (L14309). doi:10.1029/2006GL026341.
Kaus, B.J.P., Becker, T., 2007. Effects of elasticity on the Rayleigh–Taylor instability: implications for large-scale geodynamics. Geophys. J. Int. 168, 843–862. doi:10.1111/j.1365-246X.2006.03201.x.
Kreemer, C., Hammond, W.C., 2007. Geodetic constraints on areal changes in the Pacific–North America plate boundary zone: what controls basin and range extension? Geology 35, 943–947. doi:10.1130/G23868A.1.
Kostrov, B.V., 1974. Seismic moment and energy of earthquakes and seismic flow of rock. Phys. Solid Earth 1, 23–40.
Le Pichon, X., Kreemer, C., Chamot-Rooke, N., 2005. Asymmetry in elastic properties and the evolution of large continental strike-slip faults. J. Geophys. Res. 110, B03405. doi:10.1029/2004JB003343.
Luyendyk, B.P., Kamerling, M.J., Terres, R.R., Hornafius, J.S., 1985. Simple shear of southern California during Neogene time suggested by paleomagnetic declinations. J. Geophys. Res. 90, 12454–12466.
McCaffrey, R., Long, M.D., Goldfinger, C., Zwick, P.C., Nabelek, J.L., Johnson, C.K., Smith, C., 2000. Rotation and plate locking at the southern Cascadia subduction zone. Geophys. Res. Lett. 27, 3117–3120.
McCrory, P.A., 2000. Upper plate contraction north of the migrating Mendocino triple junction, northern California: Implications for partitioning of strain. Tectonics 19, 1144–1160.
Mcquarrie, N., Wernicke, B.P., 2005. An animated reconstruction of southwestern North America since 35 Ma. Geosphere 1, 147–172. doi:10.1130/GES00016.1.
Meade, B.J., Hager, B.H., 2005. Block models of crustal motion in southern California constrained by GPS measurements. J. Geophys. Res. 110, B03403. doi:10.1029/2004JB003209.
Melbourne, T., Helmberger, D., 2001. Mantle control of plate boundary deformation. Geophys. Res. Lett. 28, 4003–4006.
Moresi, L., Dufour, F., Mühlhaus, H.-B., 2003. A Lagrangian integration point finite element method for large deformation modeling of viscoelastic geomaterials. J.Comput. Phys. 184, 476–497.
Parsons, T., Sliter, R.W., Geist, E.L., Jachens, R.C., Jaffe, B.E., Foxgrover, A.C., Hart, P.E., McCarthy, J., 2003. Structure and mechanics of the Hayward–Rodgers Creek Fault step-over, San Francisco Bay, California. Bull. Seismol. Soc. Am. 93, 2187–2200.
Parsons, T., Bruns, T.R., Sliter, R., 2005. Structure and mechanics of the San Andreas–San Gregorio fault junction, San Francisco, California. Geochem. Geophys. Geosystems 6, Q01009. doi:10.1029/2004GC000838.
PBO MIT Joint Network Velocity Solution, 2007, UNAVCO, Boulder CO. Available online at: http://pboweb.unavco.org/?pageid=88, accessed January 2008, release September 2007pbo.
Prescott, W.H., Savage, J.C., Svarc, J.L., Manaker, D., 2001. Deformation across the Pacific–North American plate boundary near San Francisco, California. J. Geophys. Res. 106, 6673–6684.
Ranalli, G., 1995. Rheology of the Earth. Chapman & Hall. 413 pp.
Reasenberg, P.A., Oppenheimer, D., 1985. FPFIT, FPPLOT, & FPPAGE: Fortran computer programs for calculating & displaying earthquake fault-plane solutions. U.S. Geol. Surv. Open-File Rep, pp. 85–739.
Regenauer-Lieb, K., Weinberg, R.F., Rosenbaum, G., 2006. The effect of energy feedbacks on continental strength. Nature 442, 67–70. doi:10.1038/nature04868.
Ross, T.M., Luyendyk, B.P., Haston, R.B., 1989. Palaeomagnetic evidence for Neogene clockwise tectonic rotations in the central Mojave Desert, California. Geology 17, 470473.
Roy, M., Royden, L.H., 2000a. Crustal rheology and faulting at strike-slip boundaries. 1. An analytical model. J. Geophys. Res. 105, 5583–5597.
Roy, M., Royden, L.H., 2000b. Crustal rheology and faulting at strike-slip boundaries. 2. Effects of lower crustal flow. J. Geophys. Res. 105, 5599–5613.
Rümpker, G., Ryberg, T., Bock, G., and Desert Seismology Group, 2003. Boundary-layer mantle flow under Dead Sea transform inferred from seismic anisotropy. Nature 425, 497–501.
Savage, M.K., Fischer, K.M., Hall, C.E., 2004. Strain modelling, seismic anisotropy and coupling at strike-slip boundaries: Applications in New Zealand and the San Andreas fault. In: Grocott, J., Tikoff, B., McCaffrey, K.J.W., Taylor, G. (Eds.), Vertical Coupling and Decoupling in the Lithosphere. Geol. Soc. Lond. Spec. Pubs., 227, pp. 9–40.
Schmalzle, G., Dixon, T., Malservisi, R., Govers, R., 2006. Strain accumulation across the Carrizo segment of the San Andreas Fault, California: impact of laterally varying crustal properties. J. Geophys. Res. 111, B05403. doi:10.1029/2005JB003843.
Smith, B., Sandwell, D., 2003. Coulomb stress accumulation along the San Andreas Fault system. J. Geophys. Res. 108 (B6), 2296. doi:10.1029/2002JB002136.
Surpless, B.E., Stockli, D.F., Dumitru, T.A., Miller, E.L., 2002. Two-phase westward encroachment of basin and range extension into the northern Sierra Nevada. Tectonics 21 (1), 1002. doi:10.1029/2000TC001257.
USGS NCSN catalog, 2008. Northern California Earthquake Data Center, Berkeley CA. Available online at http://www.ncedc.org/ncedc/catalog-search.html, accessed January 2008.
Unruh, J., Humphrey, J., Barron, A., 2003. Transtensional model for the Sierra Nevada frontal fault system, eastern California. Geology 31, 327–330.
Wakabayashi, J., 1999. Distribution of displacement on and evolution of a young transform fault system: the northern San Andreas fault system, California. Tectonics 18, 1245–1274.
Wessel, P., Smith, W.H.F., 1995. New version of the generic mapping tools released. EOS Trans. AGU 76, 329.
Whitehouse, P.L., England, P.C., Houseman, G.A., 2005. A physical model for the motion of the Sierra Block relative to North America. Earth Planet. Sci. Lett. 237, 590–600.
Wilson, D.S., McCrory, P.A., Stanley, R.G., 2005. Implications of volcanism in coastal California for the Neogene deformation history of western North America. Tectonics 24, TC3008. doi:10.1029/2003TC001621.